Biochimica et Biophysica Acta 1798 (2010) 1309–1323

Contents lists available at ScienceDirect

Biochimica et Biophysica Acta

journal homepage: www.elsevier.com/locate/bbamem

Review

The action of sphingomyelinase in lipid monolayers as revealed by microscopic image analysis

Maria Laura Fanani [a,*], Steffen Hartel [b,*], Bruno Maggio [a], Luisina De Tullio [a], Jorge Jara [b], Felipe Olmos [b,c], Rafael Gustavo Oliveira [a]

[a] Departamento de Química Biológica – Centro de Investigaciones en Química Biológica de Córdoba (CIQUIBIC), Facultad de Ciencias Químicas – CONICET, Univ. Nacional de Córdoba. Haya de la Torre y Medina Allende, Ciudad Universitaria, X5000HUA, Córdoba, Argentina

[b] Laboratory for Scientific Image Processing (SCIAN-Lab, www.scian.cl), Anatomy & Developmental Biology Program, Faculty of Medicine, University of Chile, Santiago, and Nucleus of Neural Morphogenesis (NEMO), Santiago, Chile

[c] Departament of Computer Science & Departament of Mathematical Engineering, Faculty of Physical and Mathematical Sciences, University of Chile, Santiago, Chile

ARTICLE INFO

Article history:
Received 21 August 2009
Received in revised form 16 December 2009
Accepted 4 January 2010
Available online 11 January 2010

Keywords:
Sphingomyelin
Ceramide
Ceramide-enriched domain
Epifluorescence microscopy
Microscopic image processing
Active contours

ABSTRACT

In recent years, new evidence in biomembrane research brought about a holistic, supramolecular view on membrane-mediated signal transduction. The consequences of sphingomyelinase (SMase)-driven formation of ceramide (Cer) at the membrane interface involves reorganization of the lateral membrane structure of lipids and proteins from the nm to the μm level. In this review, we present recent insights about mechanisms and features of the SMase-mediated formation of Cer-enriched domains in model membranes, which have been elucidated through a combination of microscopic techniques with advanced image processing algorithms. This approach extracts subtle morphological and pattern information beyond the visual perception: since domain patterns are the consequences of subjacent biophysical properties, a reliable quantitative description of the supramolecular structure of the membrane domains yields a direct readout of biophysical properties which are difficult to determine otherwise. Most of the information about SMase action on simple lipid interfaces has arisen from monolayer studies, but the correspondence to lipid bilayer systems will also be discussed. Furthermore, the structural changes induced by sphingomyelinase action are not fully explained just by the presence of ceramide but by out-of equilibrium surface dynamics forcing the lipid domains to adopt transient supramolecular pattern with explicit interaction potentials. This rearrangement responds to a few basic physical properties like lipid mixing/demixing kinetics, electrostatic repulsion and line tension. The possible implications of such transient codes for signal transduction are discussed for SMase controlled action on lipid interfaces.

Contents

Abbreviations: SMase, Sphingomyelinase; PLA_2, phospholipase A_2; Cer, N-acylsphingosine; SM, sphingomyelin; chol, cholesterol; GUVs, giant unilamellar vesicles; ROIs, Regions of Interest; hgd, Highest Gap Distance; GGVF, generalized gradient vector flow; LE, liquid-expanded; LC, liquid-condensed; *ld*, liquid-disordered; *lo*, liquid-ordered; P^2/A, perimeter^2/area; AFM, Atomic Force Microscopy

* Corresponding authors. M.L. Fanani is to be contacted at Tel.: +54 351 4334168; fax: +54 351 4334074. S. Hartel, Tel.: +56 2 9786366.
E-mail addresses: lfanani@fcq.unc.edu.ar (M.L. Fanani), shartel@med.uchile.cl (S. Hartel).

0005-2736/$ – see front matter © 2010 Elsevier B.V. All rights reserved.
doi:10.1016/j.bbamem.2010.01.001

1. Introduction

The varied effects of the so-called "signaling lipid mediators" on the membrane structural dynamics have profound influences on the activity of lipolytic enzymes acting on membranes. This is a key aspect of molecular information exchange that represents a linking point between the local molecular events of metabolism (open to biochemical pathways) and the structural membrane dynamics (related to most functions in cell biology) [1–3]. Lipid metabolism is characterized by the fact that most substrates and products are water insoluble. Lipid substrate organization in supramolecular aggregates is essential for lipolytic enzyme efficiency and constitutes a key point in enzyme kinetics regulation [4]. As summarized in a recent review [5] phospholipase kinetics have at least four inter-dependent levels of regulation, namely: a) on the initial adsorption/partition or relocation of the enzyme in the interface; b) on the enzyme precatalytic activation that frequently determines the length of the lag period for activity; c) on the expression of catalytic activity itself through the reaction rate and d) on the extent of product formation. In addition, membrane biophysical properties undergo changes as a consequence of phospholipase action [4,6,7].

An important group of phospholipases called sphingomyelinases (SMases) hydrolyze the membrane constituent sphingomyelin (SM) to water-soluble phosphocholine and to water-insoluble ceramide (Cer). Cer is an important second messenger with unusual biophysical features such as a high tendency to segregate in liquid-condensed, Cer-enriched domains [8,9]. Cer shows strong interaction with SM and scarce miscibility with other cell membrane components [10–12]. SMase-driven aggregation of Cer-enriched domains beyond the μm scale has been identified in monolayers [13], giant liposomes (GUVs) [8], and as so-called membrane platforms in Jurkat T Cells [14]. Lateral Cer organization itself can alter physical membrane parameters like permeability [15], or introduce membrane bending that sculptures 3D membrane vesicles or apoptotic bodies [16,17]. Finally, the structural membrane reorganization itself can couple back to cellular signaling events through clustering of receptors, recruitment of intracellular signaling molecules, or exclusion of inhibitory signaling factors in Cer-enriched domains that have been reviewed in [14,18]. In summary, it has been recognized that a cellular amplifier mechanism leads from molecular activation (SMase-driven SM→Cer conversion) to self aggregated Cer-enriched domains at a supramolecular level, and structural reorganization of membrane pattern on a 2D and 3D level, all of which alter biophysical membrane parameters and couples back on receptor recruitment with the respective signal transduction down to molecular levels.

While it is becoming increasingly clear that Cer exerts a fundamental part of its physiological effects through changes in the physical properties of the membrane [19–21], details about how the kinetics of the SM→Cer conversion itself mediates morphological and pattern organization of the Cer-enriched domains have been studied by real-time monolayer approaches during the last decade [13,22,23]. As we describe in this review, the study of SMase action on lipid monolayer interfaces with Langmuir troughs coupled to quantitative time lapse fluorescence microscopy using image processing techniques has opened the access towards a more integrated view on the surprising plurality of structural and functional properties of a single enzymatic reaction.

In this context, the physiological consequences of the enzymatic production of Cer might follow similar mechanism for known members of the SMase family [6]. For availability reasons, most of the biophysical studies of SMase action reported in this review were done using bacterial enzymes. In vivo generation of Cer should be addressed in a case specific manner.

2. Enzymatic generation and visualization of Cer-enriched domains: a monolayer approach

Direct visual evidence in real time for SMase-induced formation of Cer-enriched domains was first provided by our group [13]. For this work lipid monomolecular films (monolayers) were used. Lipid monolayers provide a powerful model to study lipid–lipid and lipid–protein interactions since the thermodynamics of this system is accessible to the researcher keeping simultaneous control of molecular parameters like molecular packing, surface pressure and compressibility [24]. In addition, the Langmuir trough can be coupled to the stage of a microscope allowing the study of laterally segregated phases or domains [5,25]. When applied to the study of phosphohydrolytic reactions taking place on the membrane, this technique is unique in allowing the continuous monitoring of both the enzyme activity and the surface pattern while keeping control of organization parameters (Fig. 1). Taking advantage of the difference in cross-sectional mean molecular area occupied by SM and Cer (84 $Å^2$ and 51 $Å^2$ respectively at a surface pressure of 10 mN/m, see Fig. 1b) the time course for the SMase-driven enzymatic conversion of SM→Cer in lipid monolayers can be determined by recording the reduction of the surface area necessary to maintain a constant surface pressure (Fig. 1c and [26]). The monolayer trough allows simultaneous visualization of the monolayer by epifluorescence microscopy (Fig. 1d). Using a fluorescent probe that preferably partitions to the liquid-expanded phase, the evolution of the monolayer and domain formation can be followed in real time [13].

The use of fluorescent probes which are added to the system in study has to be handled with care, since molecular impurities, even at very low concentrations, can alter lipid mixing features like domain shape, phases extent, or even promote phase separation under specific conditions. Pioneer work by Mohwald on lipid monolayers considered the influence of impurities, like fluorescent probes on lipid domain growth [27]. More recently, a careful study by Perez-Gil's laboratory shows that the addition of 1 mol% of NBD-PC on DPPC films reduces the extent of the LC phase area up to 20% in conditions when the probe progressively accumulates in a defined area [28]. In both studies the effect is conceived as inefficiency in the phase demixing process induced by the presence of impurities. Furthermore, fluorescent probe perturbation of lipid phase segregation was also reported in bilayers. Keller's group demonstrated that the addition of as little as 0.2 mol% of $DiIC_{12}$ to DOPC/DPPC/cholesterol (chol) GUVs rises 6 °C the mixture miscibility transition temperature [29,30]. Most of these crescent evidences have been developed by means of comparison with probe-free imaging techniques. On this regards Force Microscopy, Brewster Angle Microscopy and Imaging Elipsometry have become excellent choices for the exploration of probe-free lipid monolayers or flat supported bilayers [31].

Additional consideration should be made with the extensive exposure of lipid membranes to oxidizing agents. Enlargement of liquid-ordered domains in chol/SM/phospholipid mixtures has been reported by means of the production of oxidized lipid products driven by the exposure of lipid monolayers to air [32] or by photo-oxidation in GUVs [33]. Excitation of the fluorophore in the presence of oxygen may result in peroxidation of the unsaturated bonds of membrane lipids. It was proposed that oxidized products may act either by

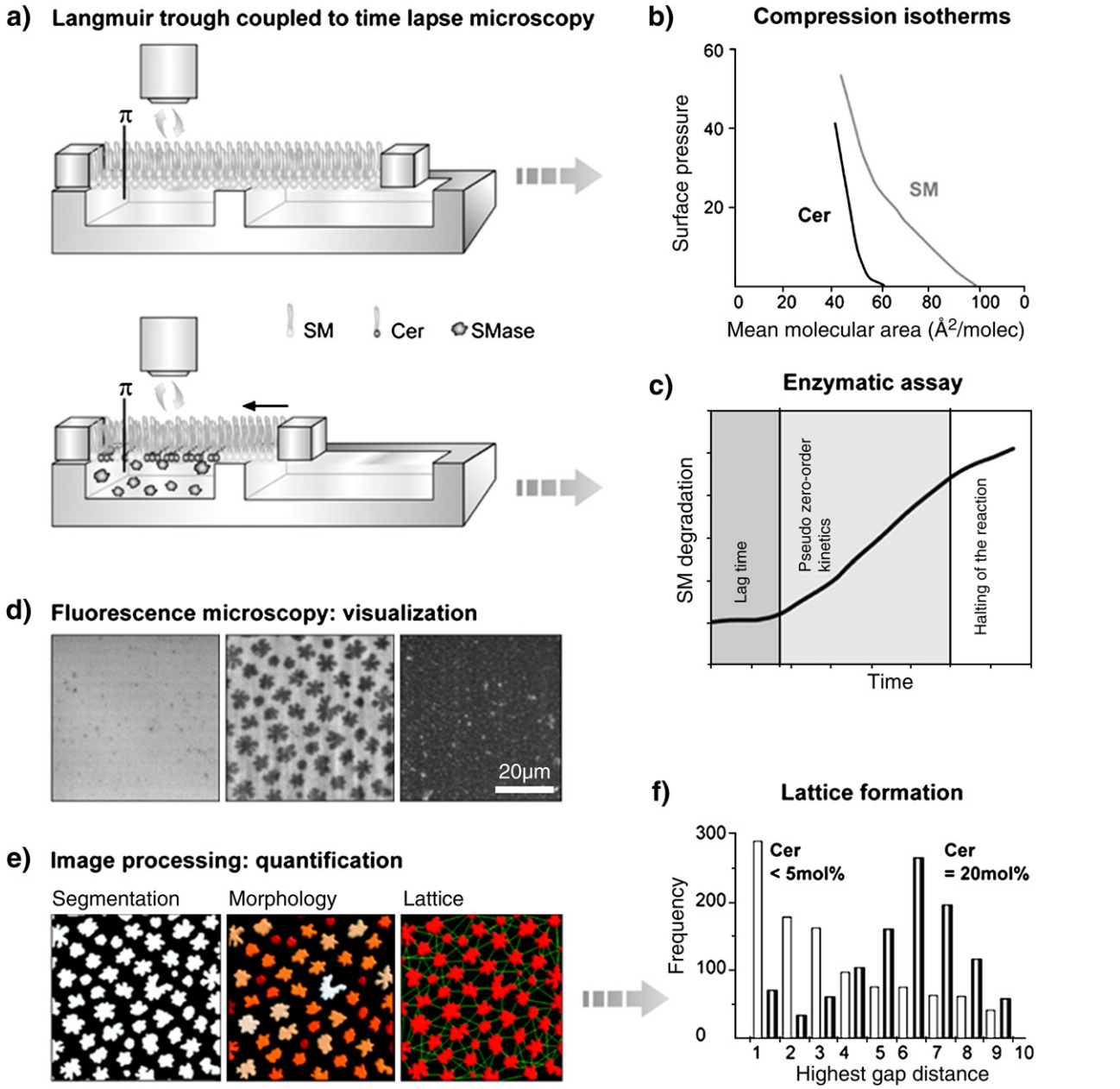

Fig. 1. Study of SMase action on lipid monolayer interfaces and quantitative time lapse microscopy through image processing. The Langmuir PTFE trough is divided into a reaction compartment and a reservoir compartment that are connected by a narrow and shallow slit to ensure surface continuity (a). After monolayer formation by deposition from an organic solvent solution of lipids, compression isotherms of the lipid monolayer can be performed for assessing molecular parameters (b). Since the product Cer occupies less area than the substrate (b), when SMase is added in the subphase of the reaction compartment, under stirring (a), the reaction progress can be followed by monitoring the barrier movement necessary to keep surface pressure constant (c). Coupling the trough to the microscope stage allows visualization of the progress of the monolayer pattern (d) from left to right fluorescence images of pure SM, SMase-treated SM monolayer, and pure Cer, doped in all cases with $DiIC_{12}$. Image processing can identify individual lipid domains as regions of interest (ROIs, white) by segmentation algorithms (e, and see Fig. 2). Segmentation leads to quantitative analysis of morphologic (center) and pattern organization (right) properties for a given domain population. Hexagonal lattice formation can be analyzed by the frequency of the highest gap distance (f). No lattices are formed for Cer concentration <5 mol% (white bars), but a preferential hexagonal lattice formation is shown for Cer = 20 mol% (black bars), which is maintained prior to percolation (see also [22]).

increasing line tension or by partitioning preferentially to the more expanded phase. For a revision on this issue see also [34].

After activation of SMase in a homogeneous, liquid-expanded (LE) SM monolayer doped with a fluorescent probe, a lag period of slow catalytic activity and unchanged surface pattern is observed (Fig. 1c–d). This lag time can last from a few seconds to tens of minutes and is strongly dependent on the enzyme concentration at the surface. During this time several kinetic processes take place involving enzyme partitioning into the interface, substrate association, a process with bimolecular kinetic dependence on the interfacial SMase, and a subsequent slow step of activation [35]. The ending of the lag time and beginning of a steady state regime is characterized by the nucleation of probe-free condensed domains that grow with the course of the SM→Cer conversion [13,22]. The morphology and composition of the Cer-enriched domains generated are strongly dependent on the reaction rate (see Section 7 and [23]). At high Cer formation rate (80% substrate degraded in <15 min) Cer-enriched domains undergo a succession of discrete morphologic transitions from circular to periodically undulating (star-like) shapes followed by a second transition toward increasingly branched morphologies. Concomitantly, interdomain superstructure organization with predominance of hexagonal domain lattices is established. Further

analysis based on theories of domain shape transitions [36], dipolar electrostatic interactions of lipid domains, and determinations of the monolayer dipole potential, reveal how these structural parameters couple to the generation of two-dimensional electrostatic fields, based upon the lipid dipole moment difference between the Cer-enriched domains and the surrounded phase. These effects revealed the significance of underlying physical properties (line tension and dipolar electrostatic repulsion) in controlling the shape of the domains and their long-range organization as outlined by [22] and Section 4. Further enrichment of Cer in SM monolayers leads to rotationally and laterally coupled domain movement before domain border contact. At this point, the condensed domains reach the percolation threshold and the liquid-expanded (probe-enriched) phase becomes discontinuous. This phenomenon is kinetically coupled to decreasing SMase activity [13,22]. Interestingly, SMase affinity for the Cer-enriched monolayers increases at this stage [35]. In summary, the detailed study of SMase activity on lipid monolayers evidences a bidirectional communication between effects taking place at the local catalytic level and the supramolecular surface organization.

3. Studying domain morphology and pattern formation with image analysis approaches

A direct visual observation of the SMase-induced formation of Cer-enriched domains can only provide a qualitative impression of the subjacent molecular processes (see supplemental movies supplied in [22]). For a quantitative approach, automated segmentation of so-called Regions of Interest (ROIs) is necessary in order to peruse morpho-topologic population statistics during the enzymatic reaction (Fig. 1e, see also Fig. 4 below). An important issue for successful segmentation of ROIs is the structure of the input data. Digital images are formed by arrays of pixels [note: considering images either uncompressed or compressed without data loss], each of them having associated a color codings or gray-scale/intensity value. Upon this scheme, several approaches for segmenting ROIs from images have been developed in recent decades, ranging from simple intensity-threshold values at pixel level to models embodying background knowledge about the objects of interest like sizes, shapes, patterns, or contour properties [37]. In 1990, Seul et al. [38] determined fluctuating domain shapes by segmentation of ROIs through the selection of intensity thresholds and application of simple chain code algorithms to obtain polygonal representations of domain boundaries in monolayers. Spectral analysis of the boundary undulations opens the access to elliptic and branching instabilities. The quantitative analysis of fluctuating domain bounder undulations, the so-called Flicker spectroscopy, has not only been applied successfully to lipid domains in monolayers, but also in GUVs [39,40]. Alternative segmentation approaches, based on threshold settings or gradient edge detectors (Canny) in combination with polygonal border representations and fast Fourier transform (FFT) have been applied recently to derive line tension in Langmuir films with high precision [41–43]. For the quantitative analysis of morpho-topological lipid domain properties in general, the quality of the segmentation algorithms which identify the ROIs on a binary level are crucial for the precision of all further methods.

To improve the quality of any segmentation procedure, image restoration algorithms like Fourier Filtering can be applied in order to remove acquisition artifacts like heterogeneous illumination or photon noise; more adequately, sophisticated deconvolution algorithms based on the physics of the acquisition process should be applied when the images are obtained near the Nyquist sampling rate, which defines the correct sampling distances (pixel or voxel dimension) for a given microscopic setup (e.g. Huygens Deconvolution Software. SVI, Hilversum, NL). Naturally, all possible pitfalls during image acquisition must be avoided in order to obtain a reliable segmentation result (see [44,45]).

In the context of Cer-enriched domains, the Nyquist criteria cannot be accomplished because of minimized fluorescence staining ($\approx$1 mol%) and fast moving domains during the exposition time of the CCD camera. We obtained reasonable results with pixel sizes of ~700 nm, which is about a factor 5 higher than the optimal Nyquist distance of ~150 nm calculated for a typical monolayer setting of a bright field microscope (20x, NA 0.8, $n=1.33$, see http://support.svi.nl/wiki/NyquistCalculator). Under these conditions, a pixel-level approach is clearly insufficient for a reliable morphological description of the domains, mainly because of the discretization effect for rounded shapes: the pixel approximation forms serrated lines for contours that do not match the horizontal or vertical pixel alignment (Fig. 2). If we compare the perimeter of a circle $p_c = 2 \cdot \pi \cdot r$ to the perimeter a pixel model of a circle $p_{pc} = 8 \cdot r$, the perimeter is overestimated by almost 30% ($4/\pi$). To avoid this problem, Freeman [46] introduced the 'Freeman Chain Code' where he classified border pixels as horizontal, diagonal, and turning points with three individual tuning parameters. While the Freeman Chain Code allows calculating ROI perimeters with errors below 5%, the curvature is estimated on the basis of a 45° code vector for each perimeter pixel. This code can only provide a rough estimation of boundary curvatures or inflection points for a given domain.

In order to optimize domain segmentation, and, at the same time, improve the parameterization of boundary curvatures and inflection points, our group implemented deformable contour models defined by geometrical curve properties that can be associated to physical parameters (Figs. 2, 3) and lead to a highly accurate contour representation of not only 2D, but also 3D lipid domains [23,47,48].

3.1. Active contour model

The parametric active contour or *snake* model [49], defines contours as time dependent parametric curves (Fig. 2). Mathematically, each contour is described by a curve C(s,t) parameterized in space by s [0,1], and in time by t [0,∞]. Two types of forces are defined in a force balance equation derived from an energy minimization principle: (i) internal forces that mimic physical contour properties and (ii) external or image forces that drive the contour towards the edges of an object. According to the dynamics defined by the force balance equation, each curve iteratively evolves from the borders of an initial, rough estimation of domain contours towards a final equilibrium shape (Fig. 2e–h). After each iteration step, the curve is re-interpolated by a set of equidistant points in order to guarantee a homogeneous parameterization and undulation of the domain border (see Fig. 2c and section below).

The terms in the balance equation are weighted by a set of force coefficients (Fig. 2), which control the final equilibrium state of the contour: a) α: coefficient for elasticity force that controls the contraction of the curve; b) β: coefficient for rigidity force that controls the bending of the curve; c) κ/q: coefficients of the image forces, generalized gradient vector flow (GGVF) and balloon force, respectively. See Section 3.3. ; d) γ: coefficient of viscosity that controls the evolution speed of the contour. The balance differential equation is integrated in time by a standard Euler method, which discretizes the time and introduces two additional parameters: (i) the time step between iterations, (Δt), and (ii) the number of iterations, ($\#t$).

3.2. Contour resolution and interpolation

In the parametric active contour model, each contour is modeled explicitly. Using xy-coordinates $[x(s,t), y(s,t)]$ R^+, the use of interpolation schemes can handle either an increasing or decreasing density of contour points. This enables a highly flexible control of the

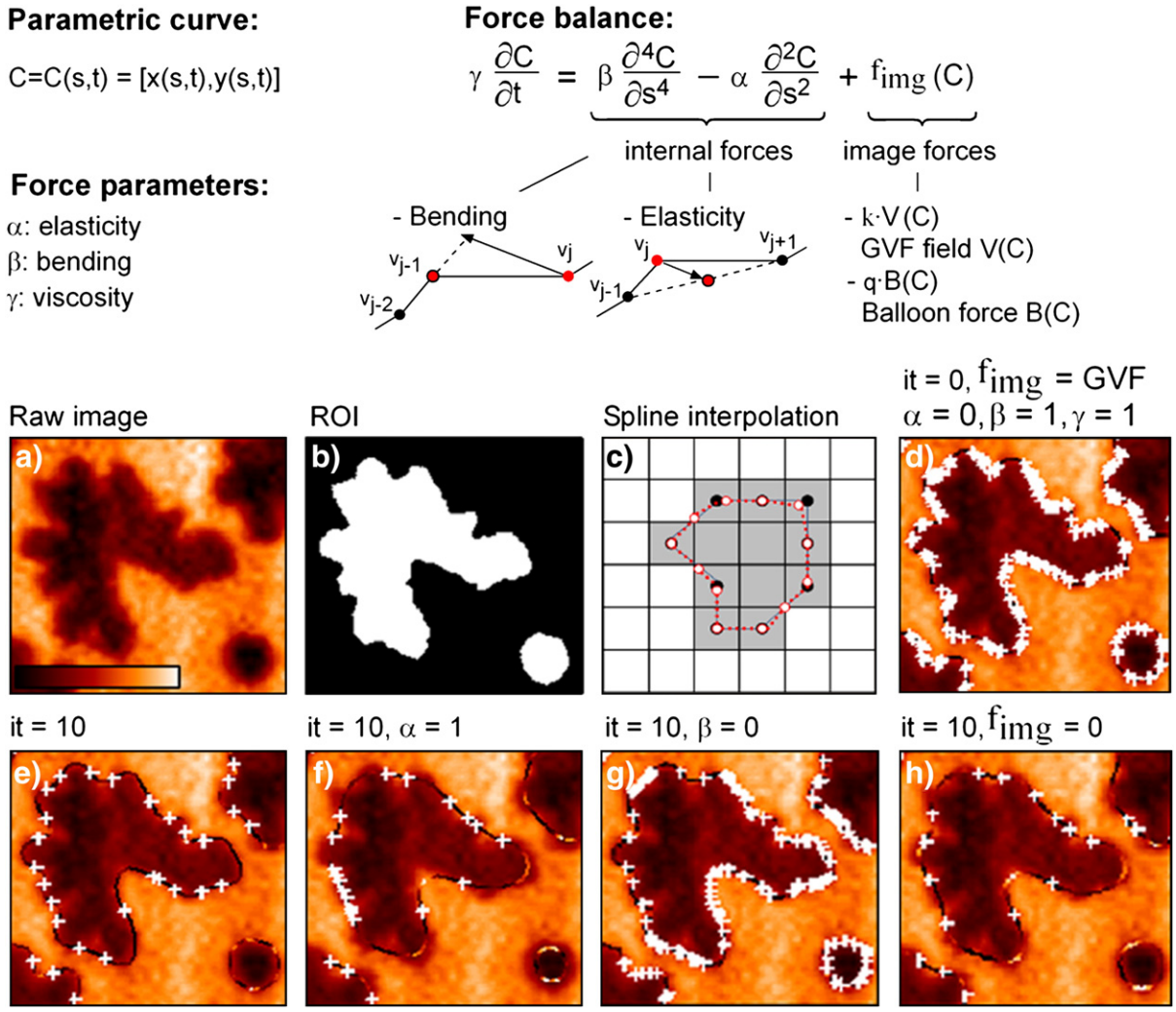

Fig. 2. Parametric active contour or 'snake' model. a) Sample image of ceramide-enriched domains using pseudo color bar. b) Threshold segmentation of the domains as Regions of Interest (ROIs). c) Spline interpolated contours: Redistribution for non-equidistant contour points (black) to equidistant interpolated points (white). d–e) Optimization of domain morphologies using the active contour approach. The initial contour at iteration step 0 (it = 0) is shown together with the indicated force parameters (d). Adjusted snake after 10 iterations (it = 10, e). Contours are drawn with pseudo colors from low to high curvature values. In d–h, white crosses mark inflection points. f–h) Adjusted snakes after 10 iterations with high elastic force coefficient ($\alpha = 1$, e), without bending force ($\beta = 0$, g), and without image forces ($f_{img} = 0$, h). All other force parameters are kept constant as outlined in d.

resolution of the Cer-domains extending an initial pixel scheme. Contour features such as perimeter and inflection points can be analyzed accurately (Fig. 2e). Two separate approaches were employed to achieve this goal: (i) a cubic spline interpolation for each contour, considering a given density of points per pixel *d* as an additional parameter for model (Fig. 2c) [23,47]; (ii) a grid approach which computes the locations of new contour points by the intersection of each contour with a grid of customizable resolution. This latter approach is capable of split or merge contours, and has been introduced as topologic adaptive snakes or 'T-snakes' [50]; its mayor advantage is that it does not depend on an initial pixel-based segmentation: the contour or contours initialize from any arbitrary contour and evolve towards a final equilibrium shape just as the original snake models.

3.3. Image forces

Image forces are computed from the original image in such a way that attracts the contours towards the domain edges. So far, two kinds of forces have been included in our approach: (i) the GGVF and (ii) balloon forces (Fig. 3). In the GGVF approach [51], an edge-map is calculated directly from the input image as a sum of the absolute intensity gradients (Fig. 3b); the gradient of this edge-map is a vector field which points in the direction of the highest local gradient (Fig. 3c). An iterative scheme is defined according to a diffusion-reaction equation, in which a flow term induces diffusion of the vector field into regions of low gradients (diffusion zones), while the vector field is conserved in regions with high gradients (edges) by an edge term. A pair of functions g and h acts as weight factors for the diffusion and the edge terms, respectively. The weight functions can also be defined to smooth noisy regions that can interfere with the evolving contours. The parameter κ weighs the GGVF in the force balance equation for the contours.

In addition to the GGVF, balloon forces [52] allow the contour to evolve properly when the vector field is not strong enough to drive the contour towards the ROI edges, which happens when the edges are too close or the contour is located in a 'plain' zone of the image (small GGVF). The intensity of the balloon force is controlled by a coefficient, *q*. To direct the balloon force, an intensity-threshold criterion is applied for each pixel, defining external and internal regions inside the image. The balloon force is oriented as a normal vector of the contour, pointing inwards if the point is located in an external zone and outwards otherwise.

In order to improve the quality of the segmentation of lipid domains successively, our approach started combining boundary detection filters with successive treatment of pixel erosion and dilatation operations

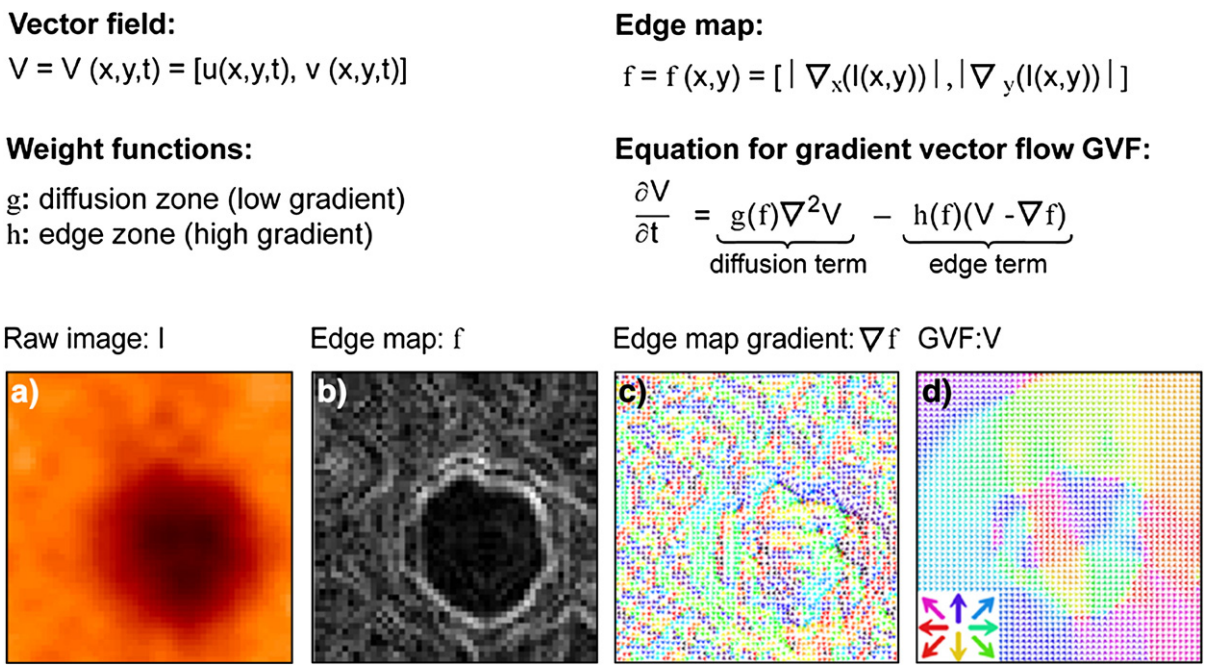

Fig. 3. Calculation of GVF forces. a) Sample image of ceramide-enriched domain using pseudo color bar. b) The edge-map *f* for the image in (a). c) The gradient of the edge-map *f*. d) The GVF field. Vectors in (c) and (d) are colored by the direction code specified at bottom left.

[13], later included Water Shed Algorithms in order to separate close domains [22], and finally included the active contour models for lipid domains in 2D [23,47]. We also expanded the concept to 3D active surfaces, which have been applied successfully for the segmentation of complex cellular and subcellular structures in the field of developmental biology [53] and 3D lipid surfaces in GUVs [48]. By choosing the appropriate model parameter combination, the domains can be segmented with high precision and the quantification of domain morphologies can be addressed reliably.

4. Domain morphology, topology, and repulsive energies

Time resolved analysis of domain morphology as presented in Fig. 4 reveals a succession of discrete stages during the pseudo-zero order kinetics of the SMase-driven SM→Cer conversion, which mark discrete shape instabilities of two-dimensional domains (modified from [22]). As can be observed, perimeter-normalized curvature drops rapidly to a final constant level. Growing Cer-enriched domains can only maintain the curvature through consecutive shape transitions to higher undulation modes m, introduced by Vanderlick and Möhwald [54]. The transition of first order to second order branching can also be observed in the example images. Cer-enriched domains adopt fractal-like shapes before percolation. The evolution of the morphology of Cer-enriched domains by SMase activity can also be characterized in terms of thermodynamic 1st and 2nd order phase transitions [55]: the spontaneous domain nucleation fulfills the criteria for a 1st order phase transition, and the conversion from circular shapes to higher harmonics belong into the category of continuous 2nd order phase transition; these shapes are topologically equivalent since they do not include discontinuities during the transitions [56]. Shape transition at t2 occurs approximately in the middle of the pseudo-zero order kinetic regime, when the shape sensitive parameter P^2/A starts to increase at a higher rate. The appearance of secondary-order branching precedes the deviation of the reaction from pseudo-zero order kinetics, signaling a marked decrease of the reaction rate, and the gradual halting of SM→Cer conversion.

Based on the theoretical treatment of harmonic shape transitions from circular domains to shapes with a higher rotation symmetry [36] or on computer simulations [54], the critical radius rm at which a circular domain becomes unstable with respect to a shape with a *m*-fold rotation symmetry is given by $rm = d \cdot e Zm \cdot e\lambda / \mu^2 / 4$. In this equation, λ is the line tension at the domain boundary, μ is the difference in the dipole moment density between the segregated lipid domains and its surrounding lipid phase, *d* is the molecular distance between neighboring dipoles, and *Zm* are shape transition exponents defined by the geometrical rotation symmetry *m*. Our approach could determine rm directly from the critical area of the domains at the point of the shape transition. The frequency of the modes *m* for the Cer-enriched domains after the first shape transition can be derived directly from the number of saddle points: $m = n/2$. The inset of Fig. 4a shows a normalized histogram for Cer-enriched domains at whose frequency values follow a Gauss like distribution which centers between $n = 12$ and 14, corresponding to $m = 6$ and 7 respectively. Using $Z_{m=6}$ according to [54] the dimensionless number $\Gamma_{SMase,\ t3'} = \mu^2/\lambda = 0.212 \pm 0.008$ relates the energy of the repulsive electrostatic interactions ($\sim\mu^2$) to the energy of the border minimizing line tension ($\sim\lambda$) which are the determinant factors for equilibrium shapes of two-dimensional lipid domains. With Γ_{SMase} and $Z_{m=0}$ for circular lipid domains in equilibrium, the theoretical equilibrium size (A_{eq}) can be calculated [22]. In conclusion, SMase generated Cer-enriched domains are characterized by an equilibrium size $A_{eq} \approx 8.8\ \mu m^2$ which lies just between the size after the spontaneous domain formation ($\approx 6\ \mu m^2$) and the critical domain size for the first shape transition ($\approx 11\ \mu m^2$).

Besides mathematical descriptors that characterize domain morphology explicitly, descriptors for the pattern organization of domain populations can reveal important details about subjacent forces. In general, a perfect lattice formation with well defined angular alignments cannot be expected in lipid monolayers. With the purpose of quantifying somewhat irregular domain lattices, the parameter highest gap distance (hgd) has shown to be a suitable classifier of lattice formation (Fig. 5a–d). Fig. 5b shows the frequency distributions of the hgd for stochastically originated model systems (Fig. 5c–d left) and for the SMase-driven experiment at two different stages of the

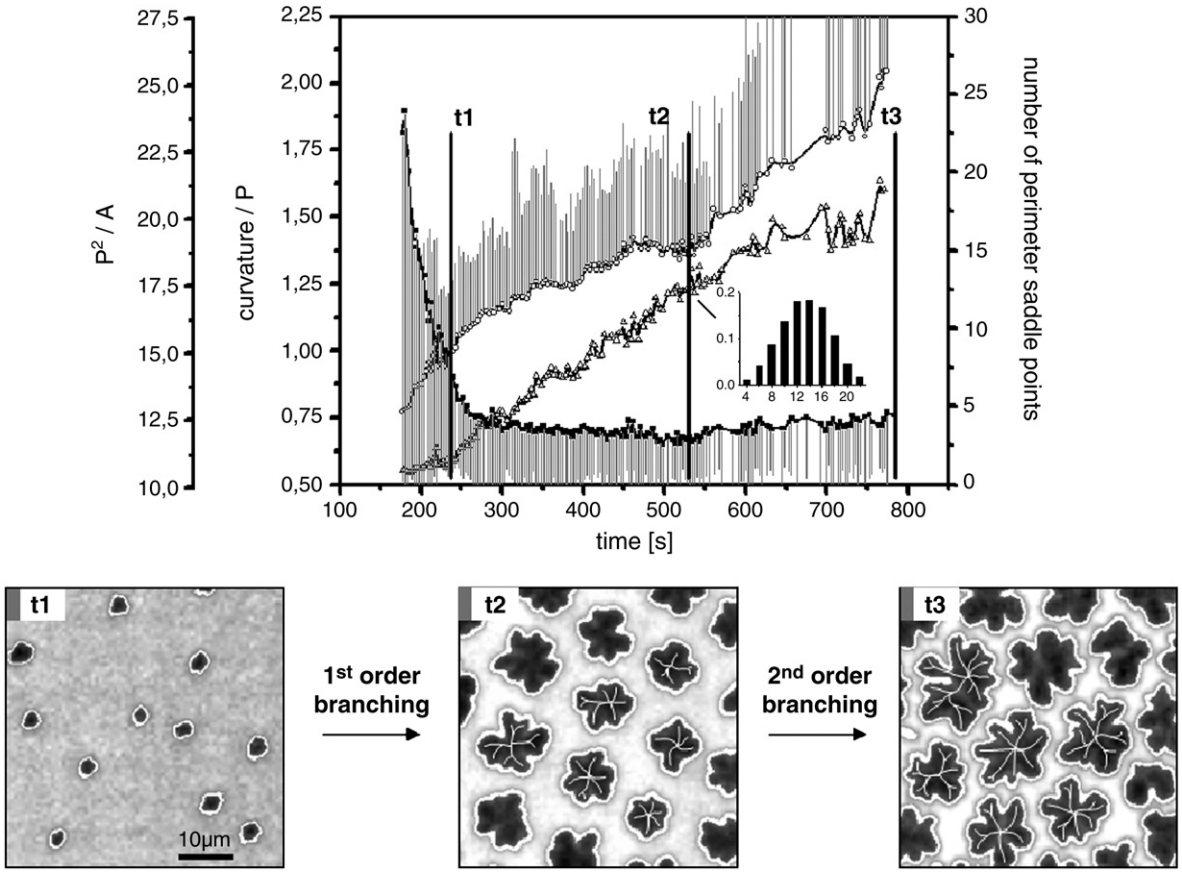

Fig. 4. Shape transitions of Cer-enriched domains during SMase-driven SM → Cer conversion. Morphologic parameters P^2/A (open circles), the curvature of the border trajectory normalized by P (closed squares), and the number of saddle points of the border trajectories (open triangle) were derived by image processed epifluorescence microscopy [modified from [22]]. At $t1$, Cer-enriched domains start to grow in a linear manner until the percolation of the domains. Error bars define SD for P^2/A and the normalized curvature. Inset shows a normalized frequency distribution of the number of perimeter saddle points from a total of 725 Cer-enriched domains at $t = t2$. Representative microscopic picture series (51.3×51.3 µm) of $DiIC_{12}$ depleted Cer-enriched domains in SM monolayers visualize morphologically discrete stages at different times of the enzymatic reaction $t1$–3. Domain borders are highlighted by white edges. As the morphologic parameters suggest, Cer-enriched domains start to grow in a circular manner until successive branching is detected at $t > t1$. Transition from first order to predominantly second order branching $t > t2$ can be detected in the plot and from the manually sketched skeletons inside the domains.

enzymatic reaction (Fig. 5c–d right). The hgd-frequency distribution confirms that the domains are randomly distributed at the beginning of the enzymatic reaction, and that SMase-driven system evolves into a predominantly hexagonal lattice pattern. While the hgd-plots (Fig. 5b) in combination with the connectivity image of domain centers (Fig. 5c–d) help to identify lattice formation, the color coded hgd-plots (Fig. 5g/h) in combination with the color coded domains (Fig. 5e/f) help to visualize lattice and even long-range pattern in form of superlattice formation. Recently, a detailed study of thermal-induced growth of solid domains on a simpler PC mixture on supported bilayers was provided by Bernchou et al. [57]. The authors correlated area, orientation, and asymmetry of lipid domains with their topology by Voronoi diagrams in binary mixture of 1,2-dioleoyl-sn-glycero-3-phosphocholine (DOPC) and 1,2-dipalmitoyl-sn-glycero-3-phosphocholine (DPPC). Similar to the SMase-driven LC domains, the PC domains also show a non-random domain lattice. The authors interpreted this finding as a consequence of the formation of a depleted region around a growing domain where the low melting PC component might become scarce. However, Bernchou et al. do not consider interdomain repulsion as a factor involved in these phenomena. On our monolayer system, lipid diffusion through the LE phase is expected to be fast enough for the depletion factor to be minimized compared to the interdomain repulsion although it may represent a second control factor for domain lattice formation. In this context, lattice formation is a direct indicator for strong repulsive energies between the lipid domains. These electrostatic energies are a consequence of differences in the dipole moment densities among the domains of the bilayer. A direct demonstration of the dipole nature of the domains in SM/Cer films was illustrated through application of external electrostatic field [58]. For experimentally determined dipole moment densities $\underline{\mu}$, the repulsive electrostatic domain energies can be calculated pixel-wise [22,59], and integrated for each domain (Fig. 6). At the beginning of the catalytic process, thermal energies which drive Brownian motion dominate over the repulsive energies among the Cer-enriched domains (Fig. 6b) which explains why random distribution has been detected for this pattern (compare Fig. 5b/c with Fig. 6a/b). At later stages, repulsive electrostatic energies increase until they dominate the random component and force the domains to adopt a predominantly hexagonal lattice (compare Fig. 5b/d with Fig. 6a/c). The energy calculations based on $\underline{\mu}$ perfectly matched the characteristics of the descriptor for lattice formation. Reversibly, hgd data allows the prediction of existing repulsive energies and hence an estimation of the differences of the domain dipole moment densities $\underline{\mu}$ for unknown scenarios. The benefit of this approach for the identification of differences between Cer-enriched domains generated by SMase activity and enzyme-free SM/Cer-mixtures will be discussed below.

5. Monolayer/bilayer correspondence

Early evidences of Cer-enriched domain formation by the action of SMase on phospholipid bilayers was provided by Kinnunen's group

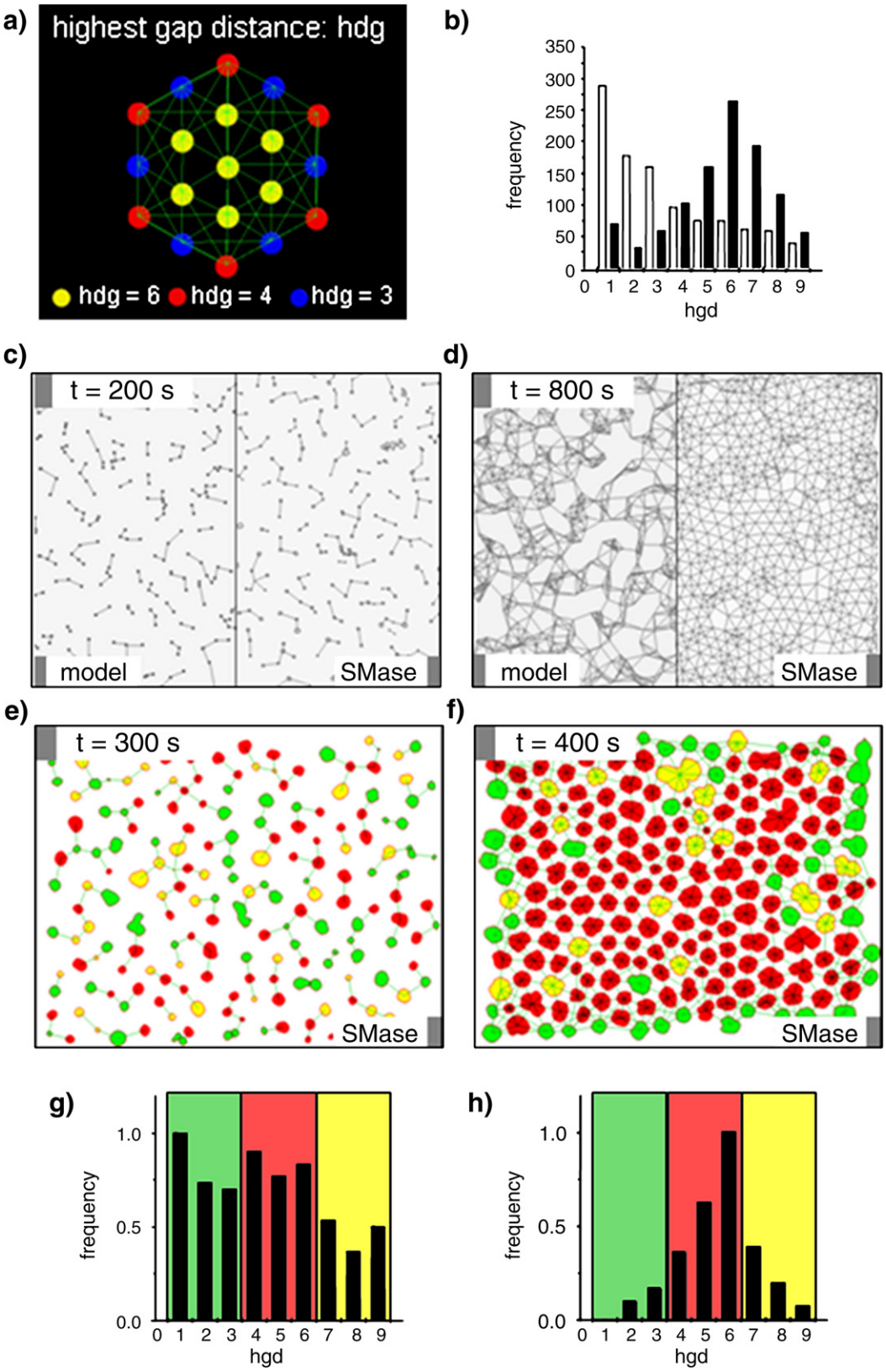

Fig. 5. Lattice formation of Cer-enriched domains during SMase-driven SM → Cer conversion (see time course in Fig. 1c). a) Visualization of the Highest Gap Distance (hgd) value, according to the algorithm of [22]. Briefly, each domain center is connected to the first 10 nearest neighbors. Euclidian distances are calculated, and sorted by length into a vector. The ranking position of the distance with the highest gap to the following distance defines the hgd of each domain. Domains embedded into hexagonal lattice are colored yellow; objects with 4 and 3 nearest neighbors are colored in blue and red. b) Frequency plot of the hgd calculated from scenarios shown in (c) and (d). White columns represent model scenarios in (c) and (left), and experimental scenario in (c) (right). Black columns represent experimental scenario in b (right). Model scenarios in (c) and (d) (left) were created by randomly seeding point sources into the image plane until the densities reach the condition of the corresponding experiments at $t = 200$ s (c) and $t = 800$ s (d) (right). (c) and (d) represent an x,y dimension of 450×354 μm. The domain centers are connected with the first (c) and the first six nearest domain centers (d), reflecting the preferential lattices formation in the SMase-driven system. e–h) Color coded Cer-enriched domains at $t = 300$ s (e) and $t = 400$ s with the corresponding hgd frequency plots (g–h). Green color marks domains with hgd = 1–3, red color hgd = 4–6 and yellow color hgd = 7–9.
Fig. 5 b–d were taken from [22], Fig. 5 a, e–h are unpublished results.

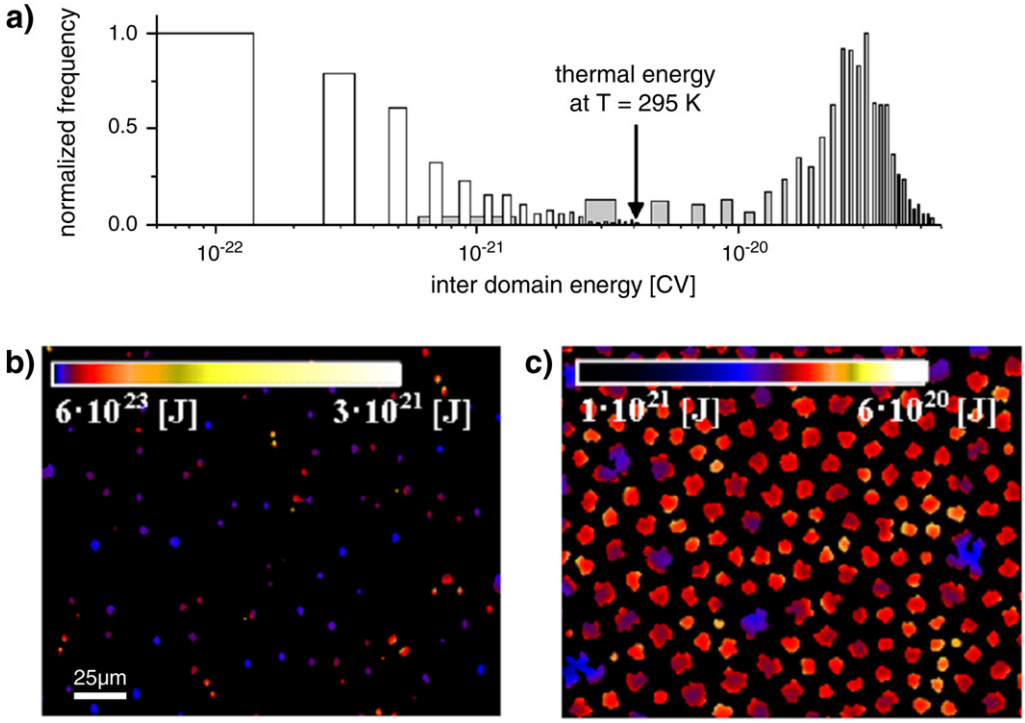

Fig. 6. Repulsive electrostatic energies between Cer-enriched domains during SMase-driven SM → Cer conversion (see time course in Fig. 1c). a) Difference of the dipole moment densities $\underline{\mu} = \underline{\mu}_{Cer} - \underline{\mu}_{SM} = 6.14 \cdot 10^{-3}$ D/Å² were calculated from the surface potential ΔV measured in pure monolayers and in defined mixtures of SM/Cer at Π = 10 mN/m and the repulsive electrostatic domain energy was calculated pixel-wise for each domain according to [22]. Frequency distribution of the repulsive electrostatic domain energies at $t = 200$ s (white columns) and $t = 450$ s (gray columns). The arrow points out the thermal energy $W(T) = 4.08 \cdot 10{-}21$ J at $T = 295$ K. b–c) Color coded presentation of the repulsive dipolar domain energies (*xy*-dimension = 225 × 176 μm).
Fig. 6 a and c were taken from [22], Fig. 6 b is an unpublished result.

[9]. The use of liposomes allowed the study of the effect of SMase action on the topological structure of the vesicle-substrate and complements monolayer studies where the topology is restricted to the plane. The addition of SMase to GUVs induces budding of smaller vesicles to the opposite side of the bilayer, evidencing the tendency of Cer to segregate in lipid domains with negative curvature [16]. Another consequence of the high negative curvature tendency of Cer is the promotion of transbilayer movement and the induction of membrane tension when Cer is enzimatically (asymmetric) formed in the bilayer [60,61].

In recent years a number of studies focused on the topographic consequence of SMase action in complex mixtures of rafts containing lipids [62–70]. Lipid rafts are putative lipid/protein microdomains occurring in cell membranes with a regulatory function on cell signaling [71]. Rafts are proposed to be lipid/protein segregated domains containing chol and sphingolipids (mainly SM) that occur in liquid-ordered (*lo*) phase surrounded by a continuous liquid-disordered (*ld*) phase. It is important to keep in mind that Cer-enriched domains are in gel phase (or its equivalent liquid-condensed (LC) phase for monolayers) and are different entities than rafts (for a recent review on Cer-enriched domain properties see [12]). Fluorescence visualization of Cer-enriched domain formation by SMase on GUVs was provided by three different laboratories [66,67,70]. These studies reported pattern reorganization when SMase is added to GUVs presenting *ld*/*lo* phase coexistence. In all cases a reduction of the extent of the *lo* phase was observed concomitant to the appearance of gel (Cer-enriched) domains. Complementarily, several independent laboratories reported almost simultaneously AFM studies on supported lipid bilayers composed by PC, chol and SM [61–63,65]. They agree in reporting the appearance of a thicker phase when treated with SMase, that was identified as Cer-enriched gel domains coexisting with *lo* (raft-like) domains on a phospholipid rich continuous phase. This behavior was also confirmed through fluorescence observation of SMase-treated supported bilayers. Chao et al. [70] reported formation of a three-phase coexistence pattern (PC-rich *ld*, SM-rich probably *lo* and Cer-rich gel phases) when SMase acts on raft lipid mixtures at short times. Similarly, Carrer et al. [69] demonstrated that the pattern reorganization shows sensitivity to the fatty acid chain composition of Cer. In this system a temporal sequence showing *ld*/*lo* coexistence → homogeneous phase → *ld*/gel coexistence was documented after SMase addition. Altogether, the above cited biophysical studies leads to the proposal that Cer formation in the cell surface would produce re-shuffling and the bringing together of molecules that were previously compartmentalized in rafts [69]. It is worth noticing that the action of SMase in bilayers (GUVs and supported bilayers) does not allow the direct estimation of the SM → Cer reaction progress; in most cases SMase action was detected only indirectly by its morphological and topographical consequences or by indirect identification with antibodies. Therefore, the correlation between the reaction progress and the membrane morphological reorganization has yet to be demonstrated in bilayers. On the other hand, a quantitative image analysis approach for domain surface areas has been recently adapted to 3D GUVs [48] opening the possibility to extent this approach to bilayers of domain morphology and dynamics as described in monolayers [22].

6. Mechanism of action of SMase at interfaces

SMase appears to be sensitive to the phase state of the substrate-membrane. Several studies both in lipid monolayers and bilayers showed an enhanced activity of SMase when the substrate is in a fluid state compared to in the gel state [26,72,73]. It is also described that SMase is modulated by the presence of a *lo* (chol-enriched) phase showing increasing activity in the order gel<*lo*<fluid phase [64,74].

Furthermore, the action of lipolytic enzymes on substrate-membranes that show phase coexistence has drawn special attention

in the context of the discussion on the function of lipid rafts. For the largely studied reaction catalyzed by phospholipase A_2 (PLA_2) several studies have related 'membrane defects', such as those arising from the coexistence of lipid domains in different physical states, with enhanced phospholipases catalytic activity [1,4,75–77]. In 1989 Salesse's group [78,79] proposed that the LE-liquid-condensed (LC) lateral interfaces (lipid domain borders) in a one-component monolayer of dipalmitoylphosphocholine (DPPC) acted as starting points for PLA_2 catalytic activity. For SMase, the presence of Cer-enriched domains in the monolayer prior to the SMase action on SM/Cer monolayers favors the activation steps in a way that is dependent on the amount of the lateral interface present as well as modulates the pattern generated by the enzyme action [47]. These results supported the strong (and generally accepted) hypothesis that lipolytic enzymes depend on physical contact at the domain boundaries in order to become fully active. This 'perimeter-activated mechanism' requires revision based on several subsequent studies.

In disagreement with the model that proposes a preferentially absorption of phospholipases to domain borders, it was reported that PLA_2 preferentially localizes in the *ld* phase in palmitoyloleoylphosphatidylcholine (POPC)/DPPC GUVs at temperatures corresponding to the gel/*ld* phase coexistence [80]. Similarly, De Tullio et al. [47] described that SMase is preferably localized in the SM-enriched LE phase of SM/Cer monolayers containing Cer-enriched (LC) domains and it does not appear enriched at the domain boundaries (Fig. 7a). They also demonstrated that the initial presence of LC domains

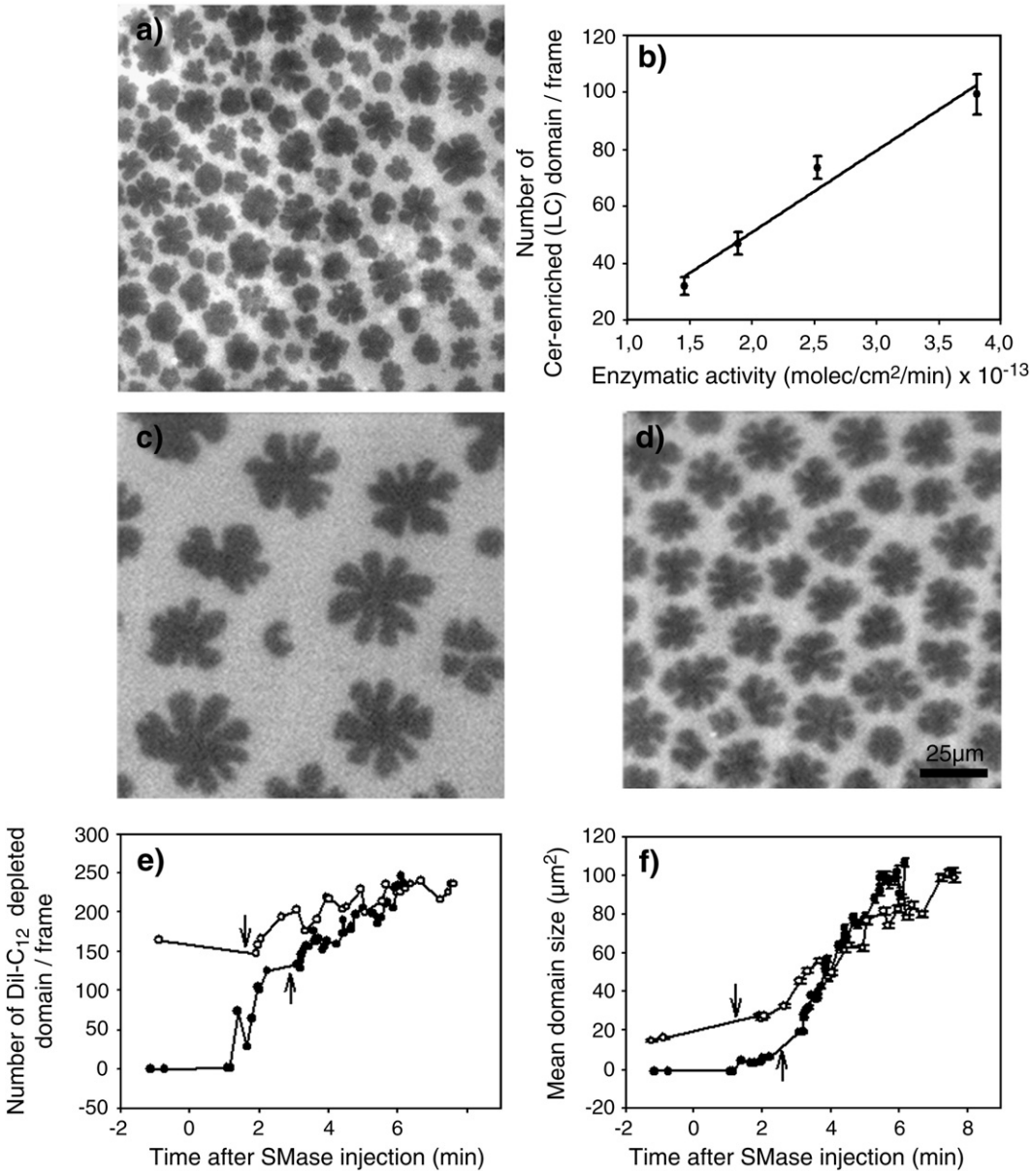

Fig. 7. SMase acts uniformly over the liquid-expanded surface on an "area-activated mechanism". (a) Surface localization of Alexa-labeled SMase acting on initially pure SM monolayers during the constant rate period showing that the labeling is not enriched at the domain borders. (b) Relationship between the number of Cer-enriched domains per frame with SMase catalytic rate. (c, d) Fluorescence representative images of initially pure SM monolayers labeled by $DiIC_{12}$ under the action of SMase (at the constant rate period) at different SMase enzymatic rates (c = 1.5 and d = 2.5 molecule/cm^2/$min^{-1} \times 10^{13}$). Image size is 140×140 µm for all panels. (e, f) Changes in the number per frame (e) and in the average size (f) of $DiIC_{12}$ depleted domains are shown as a function of time during SMase-catalyzed SM→Cer conversion. Close circles correspond to initially pure SM monolayers (homogeneous phase) and open circles to initially SM–Cer (9:1) monolayers (where Cer-enriched domains are initially present). The arrows indicate beginning of steady state regime.
Adapted from [47] and [81]. The figure in panel (a) was contrast-enhanced for better visualization, taken from Fig. 3 in [81].

regulates the kinetic parameters of the enzymatic reaction (shortening the lag time and slowing down the catalytic rate in the steady state), but do not change the pattern distribution of the enzyme [81].

The classical work by Salesse [78] interpreted that the PLA_2 catalyzed reaction starts from the lateral interface to the center of the LC domains. This interpretation arises from epifluorescence images evidencing the presence of nicks at domains edges. Nevertheless, a closer analysis reveals that the methodology cannot actually ascertain if the LE phase was not likewise degraded since substrate degradation within the LE phase is not distinguished by the probe. Furthermore, recent results from our laboratory [82] relate the presence of openings at domain sides of DPPC domains as a consequence of the kinetics of surface-mixing between substrate and products of the enzymatic reaction (DPPC vs. Lyso-PC + palmitic acid). The pattern changes observed during PLA_2 action would correspond to far-from-equilibrium mixing of products and substrate, independent on where the substrate is hydrolyzed and do not demonstrate localization of the enzyme. This concept was also explored for the SMase-catalyzed reaction resulting in out-of-equilibrium dynamic restructuring of the lipid interface forced to adopt transient supramolecular pattern (see Section 7 and [23]). Thus, the interpretation of membrane defects as starting points of hydrolytic activity should be carefully reconsidered.

Further attempts to clarify the perimeter-activated vs. the area-activated model were made by Simonsen et al. [83]. The authors followed the enzymatic hydrolysis by PLA_2 in bilayer islands in the fluid state. They concluded that their results could support that the enzyme activation occurs along the island boundaries. Nevertheless, it was also shown that both model mechanisms were able to fit the kinetic data. On the other hand, when the bilayer islands underwent discrete jumps of perimeter length but not of area, the reaction rate remained with a smooth behavior. These observations would be contrary to the perimeter-activation mechanism but can support the idea of the reaction taking place over the island surface (area-activated mechanisms).

Recently we proposed a mechanism on the basis of the area-activated hypothesis for the enzymatic action of SMase that can also explain the regulatory effect of the surface pattern [81]. SMase adsorbs homogeneously to the LE interface and exerts its catalytic activity promoting homogeneous enzymatic generation of Cer in the LE phase. Cer is partially immiscible in the SM-enriched phase [84]. When SMase acts on a uniform LE phase, the rapid production of Cer leads to a metastable, kinetically trapped, supersaturated mixed monolayer. This effect acts as driving force for the segregation of Cer-enriched domains following classical nucleation mechanisms. Nucleation process involves a certain kinetic barrier with consequences on the lengthening of the lag period before full enzymatic catalysis. The number of nucleolus that success in stabilize is dependent on the driving force for phase separation. Recently, solid domain nucleation in DOPC/DPPC bilayers was demonstrated to follow classical nucleation mechanism in cooling experiments [57]. In our system the driving force for nucleation is the extent of Cer supersaturation in the LE phase. Accordingly, the number and size of Cer-enriched domains are determined by the enzymatic rate of Cer production rather than the SMase local activity (Fig. 7b–d). When SMase exerts its action on a lipid interface that initially shows phase coexistence, the newly formed Cer molecules diffuse from the LE phase to incorporate into the Cer-enriched (pre-formed) domains. This last situation eludes Cer supersaturation in the SM-enriched phase and therefore, domain nucleation. Supporting this mechanism, SMase-treated SM/Cer monolayers show rather growing of pre-existing domains than nucleation of new domains (Fig. 7e–f) [47]. As a consequence, the kinetic barrier for nucleation is not present and the precatalytic steps can be overcome in a shorter time [81]. By this, the presence of Cer-enriched domains micrometers away from the enzyme location regulates enzyme action over a long-range. SMase catalytic activity is favored by the clearance of the product Cer from the LE (substrate) phase that diffuses to incorporate into the Cer-enriched domains. This effect promotes a low product concentration in the enzyme environment as far as Cer diffusion is faster than the Cer-production rate. This hypothesis is consistent with the finding that SMase show less activity when acting on more condensed phases (LC/gel phases or chol containing phases) [26,72,73] where Cer diffusion may be restricted [65,69]. Additionally, SMase shows an inhibited activity when acting in monolayers that initially contain Cer-enriched domains [47,85]. This may be explained by a compactness effect of the LE phase induced by the presence of Cer, demonstrated recently by AFM measured of breakthrough forces on raft lipid mixture [86].

In the light of these new evidences about the SMase mode of action at interfaces we consider important to review related data. The addition of SMase to lipid bilayers composed by the typical raft model system (DOPC/SM/chol) was reported to induce pattern reorganization by several laboratories [61,62,65,68]. The bilayers showed initially two-phase coexistence by AFM identified as PC-enriched (*ld*) and chol-enriched (*lo*) phases. The in situ generation of Cer results in the formation of thicker subdomains (Cer-enriched domains in the gel state) that are located predominantly at the edges of the *lo* domains, while the Cer-domains are located within the *lo* domains when Cer is primary incorporated (Fig. 8). This finding led to the conclusion that SMase acts primarily either at the interface between the *lo* domains-fluid phase [62] or within the *lo* domain [65]. However, taking into account the relative diffusion coefficient of the POPC enriched phase, the same data is also consistent with our area-activated hypothesis, where Cer is formed uniformly over the fluid phase and afterwards diffuse to nucleate gel domains at the *lo*–fluid phase boundary. In this case the pre-existing domain boundary would act like a nucleation seed lowering the activation energy for nucleation of the gel (Cer-enriched) phase. On the other hand, similar lipid systems (PC/SM/chol) but in free standing lipid bilayers (GUVs) that present *ld*/*lo* phase coexistence show that the action of SMase disaggregates the *lo* phase and promotes the formation of the new (Cer-enriched) gel phase [66,67,70]. Thus, the hypothesis that proposes *lo* (raft-like) domains as 'enzyme activation centers' supporting SMase action should be revised. This new model for the action of SMase, together with the finding that SMase has lower activity on the *lo* phase than on the *ld* phase [74], highlights the importance of a careful consideration of data related to raft modulation of enzymes.

7. Domain shape rearrangement as a consequence of out-of-equilibrium compositional change by SMase action

In most studies related to enzyme action and regulation, inertness of the medium, in our case the membrane, is assumed. But, active and functional membranes are far from equilibrium situations and rather present a system in a steady state condition which is controlled by fluxes of energy and matter. Consequently, thermodynamic non-equilibrium effects have direct consequences for the lateral organization of membrane components. Some authors reported that the rapid conversion of SM → Cer by SMase drives the substrate-membrane to changes in its physical properties that persist a long time after SMase halting [9,62,63,68,70]. Furthermore, several studies documented different patterns in lipid membranes that undergo enzyme-mediated production or direct incorporation of Cer to both bilayer and monolayer lipid system [13,22,62,65,69,87]. The enzymatic generation of Cer in supported lipid bilayers that show initially *ld*/*lo* phase coexistence results in the formation of gel Cer-enriched domains that are located predominantly at the edges of the *lo* domains, in contrast to the random distribution, or immersed within the *lo* domains distribution, of gel domains in bilayers where premixed Cer was incorporated (Fig. 8) [62,65]. A relatively rapid enzymatic generation (<15 min) of Cer by SMase in SM monolayers leads to a fundamentally different surface morphology and pattern organization in comparison to enzyme-free premixed SM/Cer monolayers of the

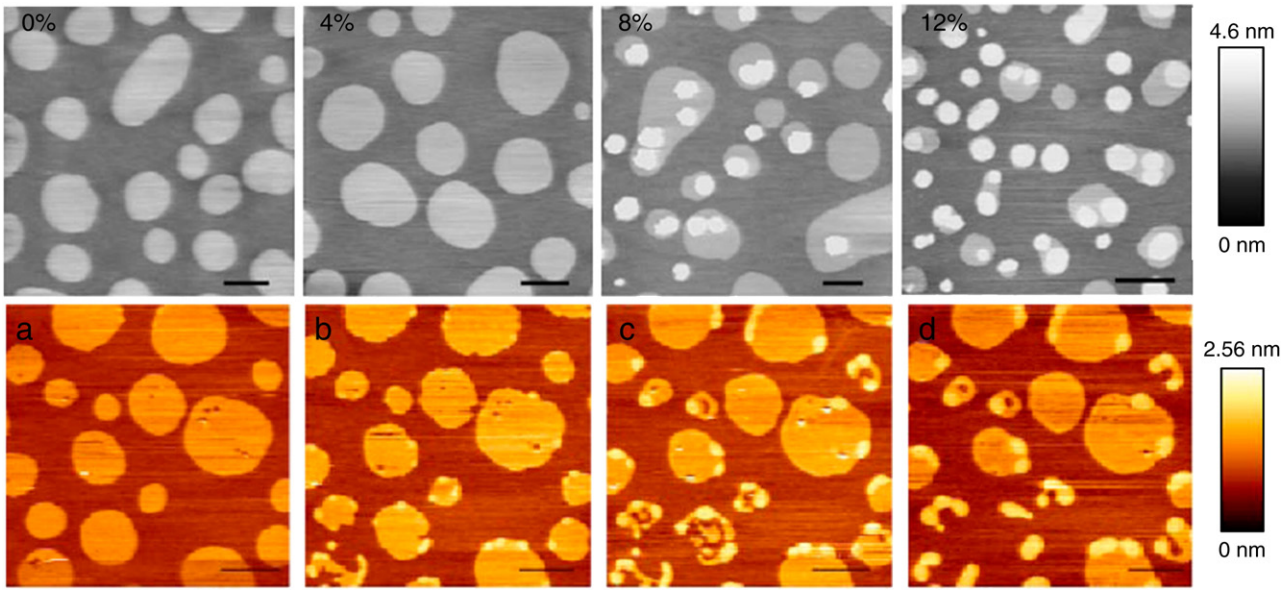

Fig. 8. AFM topographical images of supported lipid bilayers at different Cer concentrations. Upper panel: The lipid composition was DOPC:chol: (SM/Cer) 1:1:1 molar and SM was gradually substituted for Cer. In the 0% and 4% samples, two different phases with a height step of 0.8 nm can be readily distinguished. In all of the remaining images, a third topographical level can be identified at 1.2 nm above the surrounding lowest phase. Scale bar=2 μm. Lower panel: a–d show a time-course measurement on DOPC/chol/SM/:1:1:1 sample, after addition of SMase at room temperature. The enzyme was injected at the beginning of the scans represented in panels a. Imaging time was set to 4 min. Adapted from [65].

same lipid composition [13]. Detailed pattern analysis by the image processing techniques described in Section 3 revealed substantial differences in both systems [22]: i) domains formed by the action of SMase show regular sized star-like shapes while condensed rounded domains are observed in the enzyme-free films; ii) in the SMase-treated monolayer the interdomain energies force the Cer-enriched domains to adopt a predominantly hexagonal lattice formation (Fig. 5), while less ordered lattices were quantified in enzyme-free SM/Cer monolayers, and iii) only in the case of the enzyme-free SM/Cer monolayers, the LC domains formed cover an area whose relatively large size cannot be accounted by a phase of pure Cer. These differences appear the consequence of an out-of-equilibrium state of the SMase coupled monolayers. In consequence, the surface selectively 'stores' information about its genesis in form of a structural morpho-topological fingerprint.

Detailed kinetic studies of the morphological evolution of enzymatically generated Cer-enriched domains after SMase activity quenching show domain shape annealing from branched to rounded shapes with a decay halftime of about 13 min (Fig. 9). This is induced by a fast SM/Cer demixing into a LC (Cer-enriched) and LE (SM-enriched) phases. Phase separation causes a transient compositional overshoot within the LC phase that implies an increased out-of-equilibrium enrichment of Cer into the LC domains. As a consequence of the high dipole moment of the Cer molecules, electrostatic repulsion is established between domain-containing molecules leading to transient branched structures that relax to rounded shapes by lowering the proportion of Cer in the domain to equilibrium values (SM:Cer ~ 1:1) [23]. The domain shape rearrangement observed is the result of the counteraction of intradomain dipolar repulsion (favors branched/elongated structures) and line tension (favors rounded structures), according to McConnell's shape transition theory [36] and, contrary to the mechanism proposed for PC solid domain growth [57], SMase-driven Cer-enriched domains do not appear as consequence of a diffusion-limited aggregation like rapid domain growth. Thus, the system behaves as near equilibrium regarding domain shape but out-of-equilibrium regarding phases composition. In this context, the fast action of SMase can be taken as a compositional perturbation that brings about important consequences for the surface organization.

The mechanism proposed in [23] can explain the differences observed by [22] between the premixed and the enzimatically generated SM/Cer monolayers [22]: (i) domains formed by the rapid action of SMase present a higher content of Cer (close to purity), that implies higher intradomain repulsion and, as a consequence, star-like shaped domains, while condensed rounded domains formed in the enzyme-free films have lower content of Cer (close to a 1:1 SM/Cer ratio), lower μ and lower intradomain repulsion; (ii) in the SMase-treated monolayer the interdomain structuring self-organize into highly ordered hexagonal lattice patterns as a consequence of enhanced interdomain repulsion, while this repulsion is lower in enzyme-free monolayers, and (iii) in the case of the enzyme-free SM/Cer monolayers, the LC domains formed cover an area larger than that expected for the Cer content because Cer-enriched domains at equilibrium conditions also contains about 50% of SM.

Recently Chao et al. [70] described a several steps SMase-induced phase transformation. Coincident with monolayers studies, Chao's work also highlights the importance of long lasting out-of-equilibrium phase reorganization of membranes after SMase treatment. A first reorganization is observed when SMase is added to homogeneous supported bilayers composed by 40/40/20 DOPC/SM/chol. Similar to other studies [13,62,65] Cer-enriched domains are formed at short times and additionally SM-enriched (probably *lo*, chol-rich) domains also emerge. A lag time is observed until an apparent new burst of activity starts concomitant to nucleation of 3D (several microns) features enriched in all the fluorescent markers used (labeled SMase, anti-Cer antibody, Lysenin and Texas-Red DHPE). This event initiates important overall morphology reorganization of the bilayer. The authors proposed a new SMase-enriched phase, similar to the enzyme domains proposed for PLA_2 by Grainger [88]. A different interpretation could explain this phenomenon: the protein/lipid-enriched 3D features can represent nucleation of Cer (and/or chol)-induced inverted phase. Evidences of inverted phase formation after the action of SMase were provided previously in literature [89]. In this case, Chao's results may indicate an increased activity of SMase when incorporated in non-lamellar phases. Additionally, SMase action on bilayers could promote these non-lamellar structures that can up-regulate its own activity. This hypothetical mechanism

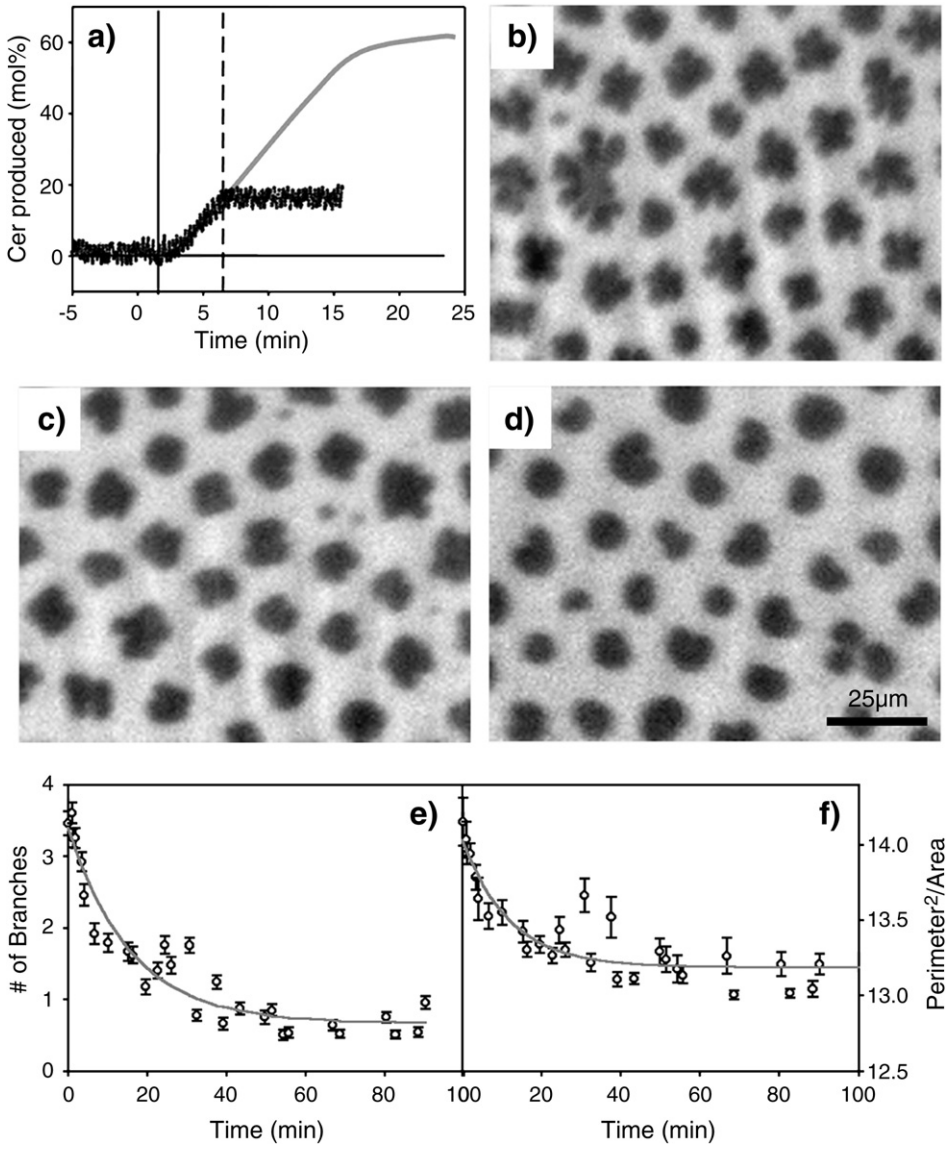

Fig. 9. Domain shape relaxation after SMase halting. (a) Time course of the SMase-catalyzed SM/Cer conversion. The solid vertical line shows the time of SMase injection into the subphase and the dashed line shows the time of SMase halting by EDTA injection into the subphase. The gray lines illustrate the time course of a similar experiment not treated with EDTA. (b–d) Epifluorescence representative images of the $DiIC_{12}$-labeled monolayer at 4, 20 and 100 min after SMase halting. Image size is 112 × 87 μm. (e–f) Time dependence of domain shape parameters: number of branches and P^2/A after SMase halting. The values correspond to averages of 100–130 domains ± SE. The gray line represents the fitted curve of the experimental data with a single exponential decay equation. All the data shown correspond to the same representative experiment.
Extracted from [23].

may represent an important regulation of SMase function on cell membrane.

The kinetics of lipid demixing (phase separation) in out-of-equilibrium situation after a sudden change of conditions represent a poorly explored field that underline some key features of the dynamic behavior of membranes [90,91]. In relation to membrane-associated enzyme activities, lipid mixing–demixing processes and the concomitant structuring of segregated domains with different lipid compositions or phase states has been shown to influence precatalytic and catalytic steps of phosphohydrolytic reactions [3,4,13,76,77,81,92]. As demonstrated for SMase, lateral enzyme-specific out-of-equilibrium organization of lipid domains represents a new level of signal transduction from local (nm) to long-range (μm) scales [23]. This cross-talk between lateral domain structures and dipolar electrostatic fields adds new and rich perspectives for the mechanisms of SMase-mediated signal transduction in biological membranes. Similarly, surface-mediated cross-talk between SMase and PLA_2 activity in monolayers, with the involvement of the respective lipid substrate and products, has been previously described [85]. In consequence, protein-driven generation of specific out-of-equilibrium states, an accepted concept for maintenance of transmembrane lipid asymmetry, should also be considered along the lateral surface.

Acknowledgements

This work was supported in part by: SECyT-UNC, MinCyT (Prov. Córdoba), CONICET and FONCyT (Argentina); some aspects of this investigation are inscribed within the PAE 22642 network in Nanobiosciences. B.M., R.G.O. and M.L.F. are Career Investigators of CONICET; L.D. is a Doctoral Fellow of CONICET. Research in SCIAN-Lab (SH) is funded by FONDECYT (1090246) and FONDEF (D07I1019), the Millennium Scientific Initiative (ICM P04-068-F). SCIAN-Lab is a selected member of the German-Chilean Center of Excellence Initiative for Medical INformatics (DAAD). JJ is funded by a PhD scholarship from CONICYT (Chile). FO is funded by FONDECYT (1090246), FONDEF (D07I1019) and Proyecto Bicentenario R18. The

Authors thank N. Contreras from Area Kreativa for support with the figures.

References

[1] R.B. Cornell, R.S. Arnold, Modulation of the activities of enzymes of membrane lipid metabolism by non-bilayer-forming lipids, Chem. Phys. Lipids 81 (1996) 215–227.
[2] F.M. Goni, A. Alonso, Structure and functional properties of diacylglycerols in membranes, Prog. Lipid Res. 38 (1999) 1–48.
[3] B. Maggio, M.L. Fanani, C.M. Rosetti, N. Wilke, Biophysics of sphingolipids II. Glycosphingolipids: an assortment of multiple structural information transducers at the membrane surface, Biochim. Biophys. Acta 1758 (2006) 1922–1944.
[4] O.G. Mouritsen, T.L. Andresen, A. Halperin, P.L. Hansen, A.F. Jakobsen, U.B. Jensen, M. Jensen, K. Jorgensen, T. Kaasgaard, C. Leidy, A.C. Simonsen, G.H. Peters, M. Weiss, Activation of interfacial enzymes at membrane surfaces, J. Phys., Condens. Matter 18 (2006) 1293–1304.
[5] B. Maggio, G.A. Borioli, B.M. Del, T.L. De, M.L. Fanani, R.G. Oliveira, C.M. Rosetti, N. Wilke, Composition-driven surface domain structuring mediated by sphingolipids and membrane-active proteins. Above the nano- but under the micro-scale: mesoscopic biochemical/structural cross-talk in biomembranes, Cell Biochem. Biophys. 50 (2008) 79–109.
[6] F.M. Goni, A. Alonso, Sphingomyelinases: enzymology and membrane activity, FEBS Lett. 531 (2002) 38–46.
[7] F.M. Goni, A. Alonso, Biophysics of sphingolipids I. Membrane properties of sphingosine, ceramides and other simple sphingolipids, Biochim. Biophys. Acta 1758 (2006) 1902–1921.
[8] R.N. Kolesnick, F.M. Goni, A. Alonso, Compartmentalization of ceramide signaling: physical foundations and biological effects, J. Cell. Physiol. 184 (2000) 285–300.
[9] J.M. Holopainen, M. Subramanian, P.K. Kinnunen, Sphingomyelinase induces lipid microdomain formation in a fluid phosphatidylcholine/sphingomyelin membrane, Biochemistry 37 (1998) 17562–17570.
[10] S.M. Alanko, K.K. Halling, S. Maunula, J.P. Slotte, B. Ramstedt, Displacement of sterols from sterol/sphingomyelin domains in fluid bilayer membranes by competing molecules, Biochim. Biophys. Acta 1715 (2005) 111–121.
[11] L.C. Silva, R.F. de Almeida, B.M. Castro, A. Fedorov, M. Prieto, Ceramide-domain formation and collapse in lipid rafts: membrane reorganization by an apoptotic lipid, Biophys. J. 92 (2007) 502–516.
[12] F.M. Goni, A. Alonso, Effects of ceramide and other simple sphingolipids on membrane lateral structure, Biochim. Biophys. Acta 1788 (2009) 169–177.
[13] M.L. Fanani, S. Hartel, R.G. Oliveira, B. Maggio, Bidirectional control of sphingomyelinase activity and surface topography in lipid monolayers, Biophys. J. 83 (2002) 3416–3424.
[14] H. Grassme, J. Riethmuller, E. Gulbins, Biological aspects of ceramide-enriched membrane domains, Prog. Lipid Res. 46 (2007) 161–170.
[15] M.B. Ruiz-Arguello, G. Basanez, F.M. Goni, A. Alonso, Different effects of enzyme-generated ceramides and diacylglycerols in phospholipid membrane fusion and leakage, J. Biol. Chem. 271 (1996) 26616–26621.
[16] J.M. Holopainen, M.I. Angelova, P.K. Kinnunen, Vectorial budding of vesicles by asymmetrical enzymatic formation of ceramide in giant liposomes, Biophys. J. 78 (2000) 830–838.
[17] A.D. Tepper, P. Ruurs, T. Wiedmer, P.J. Sims, J. Borst, W.J. van Blitterswijk, Sphingomyelin hydrolysis to ceramide during the execution phase of apoptosis results from phospholipid scrambling and alters cell-surface morphology, J. Cell Biol. 150 (2000) 155–164.
[18] C.R. Bollinger, V. Teichgraber, E. Gulbins, Ceramide-enriched membrane domains, Biochim. Biophys. Acta 1746 (2005) 284–294.
[19] F.M. Goni, F.X. Contreras, L.R. Montes, J. Sot, A. Alonso, Biophysics (and sociology) of ceramides, Biochem. Soc. Symp. (2005) 177–188.
[20] M. Schenck, A. Carpinteiro, H. Grassme, F. Lang, E. Gulbins, Ceramide: physiological and pathophysiological aspects, Arch. Biochem. Biophys. 462 (2007) 171–175.
[21] Megha, E. London, Ceramide selectively displaces cholesterol from ordered lipid domains (rafts): implications for lipid raft structure and function, J. Biol. Chem. 279 (2004) 9997–10004.
[22] S. Hartel, M.L. Fanani, B. Maggio, Shape transitions and lattice structuring of ceramide-enriched domains generated by sphingomyelinase in lipid monolayers, Biophys. J. 88 (2005) 287–304.
[23] M.L. Fanani, T.L. De, S. Hartel, J. Jara, B. Maggio, Sphingomyelinase-induced domain shape relaxation driven by out-of-equilibrium changes of composition, Biophys. J. 96 (2009) 67–76.
[24] R.E. Brown, H.L. Brockman, Using monomolecular films to characterize lipid lateral interactions, Methods Mol. Biol. 398 (2007) 41–58.
[25] V. von Tscharner, H.M. McConnell, An alternative view of phospholipid phase behavior at the air–water interface. Microscope and film balance studies, Biophys. J. 36 (1981) 409–419.
[26] M.L. Fanani, B. Maggio, Mutual modulation of sphingomyelinase and phospholipase A2 activities against mixed lipid monolayers by their lipid intermediates and glycosphingolipids, Mol. Membr. Biol. 14 (1997) 25–29.
[27] A. Miller, W. Knoll, H. Mohwald, Fractal growth of crystalline phospholipid domains in monomolecular layers, Phys. Rev. Lett. 56 (1986) 2633–2636.
[28] A. Cruz, L. Vazquez, M. Velez, J. Perez-Gil, Influence of a fluorescent probe on the nanostructure of phospholipid membranes: dipalmitoylphosphatidylcholine interfacial monolayers, Langmuir 21 (2005) 5349–5355.
[29] S.L. Veatch, S.S. Leung, R.E. Hancock, J.L. Thewalt, Fluorescent probes alter miscibility phase boundaries in ternary vesicles, J. Phys. Chem. B 111 (2007) 502–504.
[30] S.L. Veatch, S.L. Keller, Seeing spots: complex phase behavior in simple membranes, Biochim. Biophys. Acta 1746 (2005) 172–185.
[31] Physical Chemistry of Biological Interfaces, Marcel Dekker, Inc., NY, 2000.
[32] O. Coban, J. Popov, M. Burger, D. Vobornik, L.J. Johnston, Transition from nanodomains to microdomains induced by exposure of lipid monolayers to air, Biophys. J. 92 (2007) 2842–2853.
[33] A.G. Ayuyan, F.S. Cohen, Lipid peroxides promote large rafts: effects of excitation of probes in fluorescence microscopy and electrochemical reactions during vesicle formation, Biophys. J. 91 (2006) 2172–2183.
[34] L.S. Hirst, J. Yuan, The effect of fluorescent probes on model membrane organization: photo-induced lipid sorting and soft structure formation, Liq. Cryst. 36 (2009) 739–745.
[35] M.L. Fanani, B. Maggio, Kinetic steps for the hydrolysis of sphingomyelin by bacillus cereus sphingomyelinase in lipid monolayers, J. Lipid Res. 41 (2000) 1832–1840.
[36] H.M. McConnell, Harmonic shape transitions in lipid monolayer domains, J. Phys. Chem. 94 (1990) 4728–4731.
[37] K.R. Castleman, Digital Image Processing, Englewood Cliffs, NY, 1996.
[38] M. Seul, M.J. Sammon, Competing interactions and domain-shape instabilities in a monomolecular film at an air–water interface, Phys. Rev. Lett. 64 (1990) 1903–1906.
[39] C. Esposito, A. Tian, S. Melamed, C. Johnson, S.Y. Tee, T. Baumgart, Flicker spectroscopy of thermal lipid bilayer domain boundary fluctuations, Biophys. J. 93 (2007) 3169–3181.
[40] A.R. Honerkamp-Smith, P. Cicuta, M.D. Collins, S.L. Veatch, N.M. den, M. Schick, S.L. Keller, Line tensions, correlation lengths, and critical exponents in lipid membranes near critical points, Biophys. J. 95 (2008) 236–246.
[41] J.R. Wintersmith, L. Zou, A.J. Bernoff, J.C. Alexander, J.A. Mann Jr., E.E. Kooijman, E.K. Mann, Determination of interphase line tension in Langmuir films, Phys. Rev., E Stat. Nonlin. Soft Matter Phys. 75 (2007) 061605.
[42] B.L. Stottrup, A.M. Heussler, T.A. Bibelnieks, Determination of line tension in lipid monolayers by Fourier analysis of capillary waves, J. Phys. Chem. B 111 (2007) 11091–11094.
[43] M.C. Heinrich, I. Levental, H. Gelman, P.A. Janmey, T. Baumgart, Critical exponents for line tension and dipole density difference from lipid monolayer domain boundary fluctuations, J. Phys. Chem. B 112 (2008) 8063–8068.
[44] H. Pearson, The good, the bad and the ugly, Nature 447 (2007) 138–140.
[45] M.C. Brown, Fluorescence microscopy — avoiding the pitfalls, J. Cell Sci. 120 (2007) 1703–1705.
[46] H. Freeman, Boundary encoding and processing, in: B.S. Lipkin, A. Rosenfeld (Eds.), Picture Processing and Psychopictorics, Academoc Press, New York, 1990, pp. 241–266.
[47] L. De Tullio, B. Maggio, S. Hartel, J. Jara, M.L. Fanani, The initial surface composition and topography modulate sphingomyelinase-driven sphingomyelin to ceramide conversion in lipid monolayers, Cell Biochem. Biophys. 47 (2007) 169–177.
[48] M. Fidorra, A. Garcia, J.H. Ipsen, S. Hartel, L.A. Bagatolli, Lipid domains in giant unilamellar vesicles and their correspondence with equilibrium thermodynamic phases: a quantitative fluorescence microscopy imaging approach, Biochim. Biophys. Acta 1788 (2009) 2142–2149.
[49] M. Kass, A. Witkin, D. Terzopoulos, Snakes: active contour models, Int. J. Comput. Vis. 1 (1988) 321–331.
[50] T. McInerney, D. Terzopoulos, T-snakes: topology adaptive snakes, Med. Image Anal. 4 (2000) 73–91.
[51] C. Xu, J.L. Prince, Generalized gradient vector flow external forces for active contours signal processing, Signal Process. 71 (1998) 131–139.
[52] L. Cohen, On active contour models and balloons, CVGIP, Image Underst. 53 (1989) 211–218.
[53] S. Hartel, J. Jara, C.G. Lemus, M.L. Concha, 3D morpho-topological analysis of asymmetric neuronal morphogenesis in developing zebrefish, Proceedings of the International Symposium CompIMAGE 2006 — Computational Modelling of Object Represented in Images: Fundamentals, Methods and Applications, 2007, pp. 215–220.
[54] T.K. Vanderlick, H. Mohwald, Mode selection and shape transition of phospholipid monolayer domains, J. Phys. Chem. 94 (1990) 886–890.
[55] H.M. McConnell, Structures and transitions in lipid monolayers at the air–water interface, Annu. Rev. Phys. Chem. 42 (1991) 171–195.
[56] H.O. Peitgen, H. Jurgens, D. Saupe, Bausteine Des Chaos, (Ed.), Fraktale, Rowohld GmbH, Hamburg, 1998, 129.
[57] U. Bernchou, J.H. Ipsen, A.C. Simonsen, Growth of solid domains in model membranes: quantitative image analysis reveals a strong correlation between domain shape and spatial position, J. Phys. Chem. B 113 (2009) 7170–7177.
[58] N. Wilke, B. Maggio, Effect of externally applied electrostatic fields on the surface topography of ceramide-enriched domains in mixed monolayers with sphingomyelin, Biophys. Chem. 122 (2006) 36–42.
[59] P. Nassoy, W.R. Birch, D. Andelman, F. Rondelez, Hydrodynamic mapping of two-dimensional electric fields in monolayers, Phys. Rev. Lett. 76 (1996) 455–458.
[60] F.X. Contreras, A.V. Villar, A. Alonso, R.N. Kolesnick, F.M. Goni, Sphingomyelinase activity causes transbilayer lipid translocation in model and cell membranes, J. Biol. Chem. 278 (2003) 37169–37174.
[61] I. Lopez-Montero, M. Velez, P.F. Devaux, Surface tension induced by sphingomyelin to ceramide conversion in lipid membranes, Biochim. Biophys. Acta 1768 (2007) 553–561.
[62] Ira, L.J. Johnston, Ceramide promotes restructuring of model raft membranes, Langmuir 22 (2006) 11284–11289.

[63] Ira, L.J. Johnston, Sphingomyelinase generation of ceramide promotes clustering of nanoscale domains in supported bilayer membranes, Biochim. Biophys. Acta 1778 (2008) 185–197.
[64] L.C. Silva, A.H. Futerman, M. Prieto, Lipid raft composition modulates sphingomyelinase activity and ceramide-induced membrane physical alterations, Biophys. J. 96 (2009) 3210–3222.
[65] S. Chiantia, N. Kahya, J. Ries, P. Schwille, Effects of ceramide on liquid-ordered domains investigated by simultaneous AFM and FCS, Biophys. J. 90 (2006) 4500–4508.
[66] Y. Taniguchi, T. Ohba, H. Miyata, K. Ohki, Rapid phase change of lipid microdomains in giant vesicles induced by conversion of sphingomyelin to ceramide, Biochim. Biophys. Acta 1758 (2006) 145–153.
[67] G. Staneva, A. Momchilova, C. Wolf, P.J. Quinn, K. Koumanov, Membrane microdomains: role of ceramides in the maintenance of their structure and functions, Biochim. Biophys. Acta 1788 (2009) 666–675.
[68] Ira, S. Zou, D.M. Ramirez, S. Vanderlip, W. Ogilvie, Z.J. Jakubek, L.J. Johnston, Enzymatic generation of ceramide induces membrane restructuring: correlated AFM and fluorescence imaging of supported bilayers, J. Struct. Biol. 168 (2009) 78–89.
[69] D.C. Carrer, E. Kummer, G. Chwastek, S. Chiantia, P. Schwille, Asymmetry determines the effects of natural caramides on model membranes, Soft Matter 5 (2009) 3279–3286.
[70] L. Chao, A.P. Gast, T.A. Hatton, K.F. Jensen, Sphingomyelinase-induced phase transformations: causing morphology switches and multiple-time-domain ceramide generation in model raft membranes, Langmuir 26 (2010) 344–356.
[71] M. Edidin, The state of lipid rafts: from model membranes to cells, Annu. Rev. Biophys. Biomol. Struct. 32 (2003) 257–283.
[72] M. Jungner, H. Ohvo, J.P. Slotte, Interfacial regulation of bacterial sphingomyelinase activity, Biochim. Biophys. Acta 1344 (1997) 230–240.
[73] M.B. Ruiz-Arguello, M.P. Veiga, J.L. Arrondo, F.M. Goni, A. Alonso, Sphingomyelinase cleavage of sphingomyelin in pure and mixed lipid membranes. Influence of the physical state of the sphingolipid, Chem. Phys. Lipids 114 (2002) 11–20.
[74] F.X. Contreras, J. Sot, M.B. Ruiz-Arguello, A. Alonso, F.M. Goni, Cholesterol modulation of sphingomyelinase activity at physiological temperatures, Chem. Phys. Lipids 130 (2004) 127–134.
[75] B. Maggio, Control by ganglioside GD1a of phospholipase A2 activity through modulation of the lamellar-hexagonal (HII) phase transition, Mol. Membr. Biol. 13 (1996) 109–112.
[76] C. Leidy, L. Linderoth, T.L. Andresen, O.G. Mouritsen, K. Jorgensen, G.H. Peters, Domain-induced activation of human phospholipase A2 type IIA: local versus global lipid composition, Biophys. J. 90 (2006) 3165–3175.
[77] W.R. Burack, Q. Yuan, R.L. Biltonen, Role of lateral phase separation in the modulation of phospholipase A2 activity, Biochemistry 32 (1993) 583–589.
[78] D.W. Grainger, A. Reichert, H. Ringsdorf, C. Salesse, An enzyme caught in action: direct imaging of hydrolytic function and domain formation of phospholipase A_2 in phosphatidulcholine monolayers, FEBS Lett. 252 (1989) 73–82.
[79] D.W. Grainger, A. Reichert, H. Ringsdorf, C. Salesse, D.E. Davies, J.B. Lloyd, Mixed monolayers of natural and polymeric phospholipids: structural characterization by physical and enzymatic methods, Biochim. Biophys. Acta 1022 (1990) 146–154.
[80] S.A. Sanchez, L.A. Bagatolli, E. Gratton, T.L. Hazlett, A two-photon view of an enzyme at work: Crotalus atrox venom PLA2 interaction with single-lipid and mixed-lipid giant unilamellar vesicles, Biophys. J. 82 (2002) 2232–2243.
[81] L. De Tullio, B. Maggio, M.L. Fanani, Sphingomyelinase acts by an area-activated mechanism on the liquid-expanded phase of sphingomyelin monolayers, J. Lipid Res. 49 (2008) 2347–2355.
[82] L. De Tullio, B. Maggio, Regulación De La Estructura y Dinámica De La Topografía De Superficie Por Enzimas Lipolíticas, Univ.Nac.Cordoba, Cordoba, Argentina, 2009.
[83] A.C. Simonsen, U.B. Jensen, P.L. Hansen, Hydrolysis of fluid supported membrane islands by phospholipase A(2): time-lapse imaging and kinetic analysis, J. Colloid Interface Sci. 301 (2006) 107–115.
[84] J.V. Busto, M.L. Fanani, T.L. De, J. Sot, B. Maggio, F.M. Goni, A. Alonso, Coexistence of immiscible mixtures of palmitoylsphingomyelin and palmitoylceramide in monolayers and bilayers, Biophys. J. 97 (2009) 2717–2726.
[85] M.L. Fanani, B. Maggio, Surface pressure-dependent cross-modulation of sphingomyelinase and phospholipase A2 in monolayers, Lipids 33 (1998) 1079–1087.
[86] R.M. Sullan, J.K. Li, S. Zou, Direct correlation of structures and nanomechanical properties of multicomponent lipid bilayers, Langmuir 25 (2009) 7471–7477.
[87] L.R. Montes, M.B. Ruiz-Arguello, F.M. Goni, A. Alonso, Membrane restructuring via ceramide results in enhanced solute efflux, J. Biol. Chem. 277 (2002) 11788–11794.
[88] D.W. Grainger, A. Reichert, H. Ringsdorf, C. Salesse, Hydrolytic action of phospholipase A2 in monolayers in the phase transition region: direct observation of enzyme domain formation using fluorescence microscopy, Biochim. Biophys. Acta 1023 (1990) 365–379.
[89] F.X. Contreras, G. Basanez, A. Alonso, A. Herrmann, F.M. Goni, Asymmetric addition of ceramides but not dihydroceramides promotes transbilayer (flip-flop) lipid motion in membranes, Biophys. J. 88 (2005) 348–359.
[90] K. Jorgensen, A. Klinger, R.L. Biltonen, Nonequilibrium lipid domain growth in the gel-fluid two-phase region of a DC16PC-DC22PC lipid mixture investigated by Monte Carlo computer simulation, FT-IR, and fluorescence spectroscopy, J. Phys. Chem. B 104 (2000) 11763–11773.
[91] R.F. de Almeida, L.M. Loura, A. Fedorov, M. Prieto, Nonequilibrium phenomena in the phase separation of a two-component lipid bilayer, Biophys. J. 82 (2002) 823–834.
[92] H.W. Huang, E.M. Goldberg, R. Zidovetzki, Ceramide induces structural defects into phosphatidylcholine bilayers and activates phospholipase A2, Biochem. Biophys. Res. Commun. 220 (1996) 834–838.